Minimization of instabilities in growing interfaces: A variational approach

Eduardo O. Dias and José A. Miranda*

Departamento de Física, Universidade Federal de Pernambuco, Recife, Pernambuco 50670-901, Brazil

(Received 3 September 2013; revised manuscript received 28 October 2013; published 19 December 2013)

The Mullins-Sekerka and the electric breakdown instabilities are well known to lead to the spontaneous formation of a variety of complex spatial structures, among them dendritic crystal shapes, and treelike electric discharge patterns. Controlling such systems by suppressing predominantly excited solutions offers the opportunity to manipulate and stabilize these patterns in a defined way for a wide range of technological applications. In this work, we employ a variational approach which enables one to systematically search for the ideal conditions under which the patterns grow, but where interfacial deformations are efficiently minimized. The effectiveness of our variational control method is illustrated via linear stability calculations on both two-dimensional and three-dimensional contour-dynamics models for crystal growth and electric discharge phenomena.

DOI: 10.1103/PhysRevE.88.062404 PACS number(s): 81.10.Aj, 51.50.+v, 47.54.−r, 47.15.gp

I. INTRODUCTION

The formation of patterns and shapes in the natural world has long been a source of fascination for both scientists and laymen [1,2]. Nature provides an endless array of patterns formed by diverse physical, chemical, and biological systems [3]. The scales of such patterns range from the growth of bacterial colonies [4] to the large-scale structure of the universe [5]. This enormous range of scales over which pattern formation occurs and the intriguing fact that they emerge spontaneously from an orderless and homogeneous environment captivate our imagination.

Interface dynamics plays a major role in spontaneous pattern formation in nature. It determines the shapes of objects, and therefore it has important applications in a wide range of interdisciplinary fields: hydrodynamics [6] (convection patterns and shapes of boundaries between fluids), metallurgy [7] (dendritic shapes of crystals), and biology [4,8] (shapes of plants, cells, etc.). Despite the great variety and richness of this immense set of pattern formation systems, in this work we concentrate on a few illustrative, but important examples of interfacial patterns. Actually, instead of focusing on studying the development of patterns, our main goal is to offer ways to control their growth.

One paradigmatic system in the area of interfacial pattern formation is the Saffman-Taylor (viscous fingering) problem [9], in which fingering structures arise at the boundary separating two fluids of differing viscosities, when they move in the narrow gap between parallel glass plates (a device named the Hele-Shaw cell [10]). From the dynamic interaction between capillary and viscous forces ones has the formation of interface shapes which can vary from a steady single-fingered pattern to convoluted fronts in which fingerlike structures split at their tips, tending towards a dense-branching morphology. This fluid dynamic problem has been actively studied over half a century [11], and is an archetype for a wide range of fields, including research in oil recovery processes [12], fluid mixing [13], flow in granular media [14], microdischarges in plasmas [15], and biodynamics of cell fragmentation [16,17].

Distinct, but related types of interfacial patterns are formed in other physical systems. Two particular examples have received considerable attention over the past several years: (i) dendritic growth of a solid from a melt [18,19], linked to the celebrated Mullins-Sekerka instability [20–29]; (ii) the electric breakdown problem that studies the uprise and propagation of ionization waves through electric discharges [30–36]. These two systems and the viscous fingering problem have the common feature that there exists a moving boundary between two phases, on which competing stabilizing and destabilizing forces act. It is the interplay between these forces that controls the dynamic evolution of the complex patterns.

The main physical mechanisms involved in the interfacial pattern formation problem of Mullins-Sekerka, and in electric discharges can be briefly described as follows. Regarding the Mullins-Sekerka instability, we focus on the simplest example of the solidification of a pure substance from its melt [18–21]. In the conventional thermodynamic model, the fundamental rate-controlling mechanism is the diffusion of latent heat away from the interface between the liquid and the solid phases. If the solid develops an outward bump on the solid-melt interface, the temperature gradient is larger there. This happens because the supercooling temperature difference is applied across a shorter length. As a result, the diffusion of latent heat away into the melt is larger at the bump, and it grows faster. If a bump becomes too sharp, however, it tends to melt back because of surface tension (the equilibrium melting temperature of a solid is reduced proportionally to the interface curvature [18–21]). The competition between these two opposing effects leads to a morphologically unstable process which characteristically produces dendrites or snowflake-like structures. In addition to these competing factors, an important third player in this game is anisotropy. The average bonding energy between atoms at the interface depends on the orientation of the interface relative to internal crystal axes. So, anisotropy is required in the interfacial dynamics to produce typical dendritic growth. Similarly, in the simplest hydrodynamic-like approximation [34], the ionization fronts in the electric discharge problem are subjected to stabilizing forces due to diffusion which tend to dampen out any disturbances, and to destabilizing forces due to electric field. The competition between these two factors

*jme@df.ufpe.br

result in the typical treelike patterns formed during electric discharges.

Despite their visual appeal and considerable interest from both academic and applied points of view, the emergence of intricate pattern-forming shapes is not always desirable. For instance, it is well known that viscous fingering is a major factor in reducing oil recovery from underground petroleum reservoirs [12]. Something similar occurs in crystal growth problems, more precisely in crystal casting applications [27], where it is advantageous to suppress the Mullins-Sekerka instability and prevent the formation of dendrites. Finally, it is also known that many industrial techniques (e.g., water purification, chemical processing of gases, etc.) could be improved if the emergence of treelike patterns due to electric discharges could be controlled or avoided [36]. Therefore, it is of scientific and technological importance to investigate how to control, minimize, and possibly suppress the growth of all these interfacial instabilities.

Recently, we have tackled the problem of restraining the viscous fingering instability in radial, quasi-two-dimensional Hele-Shaw cells [37]. We have devised an analytical variational scheme which allowed us to find the ideal injection rate that would lead to a pattern evolution in which interfacial disturbances could be properly minimized. The effectiveness of our variational controlling protocol for the radial Saffman-Taylor problem has been substantiated by both experiments and numerical simulations. Motivated by these facts, in this work, we use our variational scheme to try to minimize the development of interfacial disturbances in the Mullins-Sekerka instability and in the electric breakdown problem. More specifically, the variational method is employed to systematically search for the particular functional forms for the far-field heat flux or far-field temperature (in the Mullins-Sekerka case), and for the electric charge or current (in the electric discharge situation) that result in the minimization of interfacial perturbations. This provides simple and practical ways, derived from first principles, to improve the efficiency and control of the pattern formation events in these two physically important systems.

Our present study extends the previous variational results originally obtained for the control of the effectively two-dimensional viscous fingering problem [37] in a few different directions. First, we apply the minimization process to two new systems of great scientific and technological appeal (crystal growth and electric discharges). Notice that, despite the phenomenological proximity in the description of the physical competition mechanisms leading to these distinct interfacial instability problems, *a priori*, from the results of Ref. [37] one just cannot tell for sure what would be the precise controlling flux (of heat, or charge) that would lead to minimization of interfacial irregularities in these two new systems. Moreover, in contrast to what was done in [37], in this work our calculations are performed for both two-dimensional and fully three-dimensional versions of the problems. The change in the problems' dimensionality add new components into the calculations, and poses difficulties in any presumptive accurate prediction about the ideal controlling protocols for these cases. Moreover, the inclusion of three-dimensional contributions may provide a closer connection between our theoretical results with associated real life growth processes.

II. VARIATIONAL METHOD AND PHYSICAL APPLICATIONS

A. Variational method

Consider the two-dimensional growth of a perturbed interface separating two phases, described as

$$\mathcal{R}(\theta,t) = R(t) + \zeta(\theta,t), \tag{1}$$

where

$$\zeta(\theta,t) = \sum_{n\neq 0} \zeta_n(t) \exp(in\theta) \tag{2}$$

represents the net interfacial perturbation in polar coordinates (r,θ) with Fourier amplitudes $\zeta_n(t)$, and discrete azimuthal wave numbers n. $R = R(t)$ is the time-dependent unperturbed radius of the interface and R_0 is its radius at initial time $t = t_0$. The linear perturbation amplitude evolves in time according to [20,35,38]

$$\zeta_n(t) = \zeta_n(0) \exp\{I(n,R,\dot{R})\} \tag{3}$$

with

$$I(n,R,\dot{R}) = \int_{t_0}^{t} \lambda(n,R,\dot{R})dt, \tag{4}$$

$\zeta_n(0)$ being the interfacial amplitude at $t = t_0$, and $\lambda(n,R,\dot{R})$ the linear growth rate. The overdot denotes total time derivative. An important information from the linear analysis is the mode of maximum growth rate $n_{\max}$ which can be calculated by setting $d\lambda(n,R,\dot{R})/dn = 0$.

As commented in Sec. I, an efficient method to control interface instabilities has been recently proposed in Ref. [37], and successfully tested for the injection-induced radial viscous fingering case. The main task of this approach is minimizing the perturbations amplitudes (3). This can be accomplished by extremizing the integral (4). Since $n_{\max}$ is the fastest growing mode, the method focus on minimizing the integral

$$I(n_{\max},R,\dot{R}) = \int_{0}^{t} \lambda(R,\dot{R})dt', \tag{5}$$

where $t_0 = 0$. Notice that $\lambda(n_{\max},R,\dot{R}) = \lambda(R,\dot{R})$ only depends on R and $\dot{R}$. So, if the interface evolves from a fixed initial and final radii, during a time interval $[0,t_f]$ we have a variational problem, in which I in Eq. (5) represents the *action*, while λ defines the *Lagrangian* of the system. This can be solved by using the Euler-Lagrange equation

$$\frac{d}{dt}\left(\frac{\partial\lambda}{\partial\dot{R}}\right) = \frac{\partial\lambda}{\partial R}, \tag{6}$$

with fixed endpoints $R(t=0) = R_0$ and $R(t=t_f) = R_f$. Substituting the growth rate into Eq. (6) we obtain the differential equation that describes how the radius $R(t)$ must vary in time in order to minimize the interface instabilities described by Eq. (2).

Before we proceed an important clarification must be given: despite its simplicity, the minimization procedure described above does not provide a rigorous mathematical proof that it really provides the true optimum minimum of the problem. Note that our main approximation is that we minimize the integral $I(n_{\max},R,\dot{R})$ [see Eq. (5), where $n = n_{\max}$], and not

the maximum of $I(n,R,\dot{R})$ with respect to $R(\{n\},t)$, which is a much more difficult task. On the other hand, the validity of our simplified theoretical minimization procedure has been substantiated by laboratory experiments and fully nonlinear numerical simulations in Ref. [37] for the viscous fingering problem. These facts support the idea that despite of the fact that our minimization procedure may not lead to the exact true optimum of the problem, it does offer a useful and simple approximation to it. So, in this work whenever we mention the optimal (or, ideal) flux rate we refer to it in the context of our simplified minimization method.

In the next two sections we will apply this variational approach to two fundamental interface instability problems: (i) *crystal growth* and (ii) *electric discharge*. In both systems we obtain fairly simple solutions for Eq. (6) allowing us to verify analytically the efficacy of our variational controlling strategy.

B. Minimization of instabilities in the crystal growth process

Consider a quasistatic growth of a solid (phase 1) in a supercooled liquid (phase 2), of temperatures T_1 and T_2 [20–27], respectively. By admitting that the thermal diffusivities of the phases are identical, and that the local equilibrium holds at the interface, the dimensionless equations of the problem are [24–27]

$$\begin{aligned} &\nabla^2 T_i = 0, \quad i = 1,2, \\ &\mathbf{v} = [\nabla T_1 - \nabla T_2]|_{r=\mathcal{R}}, \quad T_i|_{r=\mathcal{R}} = -\tau(\mathbf{n})\kappa, \\ &J = \frac{1}{2\pi}\int_{r=\mathcal{R}} \mathbf{n}\cdot\mathbf{v}\, ds, \quad \left(\frac{d\mathbf{r}}{dt}\right)_{r=\mathcal{R}} = \mathbf{v}. \end{aligned} \tag{7}$$

where T_i is the temperature field ($i = 1$ or 2 for solid and liquid phases, respectively), $\mathbf{v}$ is the velocity of the interface, $\mathbf{n}$ is the unit normal vector to the interface, τ is the anisotropic surface tension, J is the far-field heat flux, and κ is the interface curvature. Here we neglected kinetic effects in the third expression of Eqs. (7). Note that J specifies the time derivative of the solid phase area (or volume). In the three-dimensional case the factor of $1/2\pi$ is replaced by $1/4\pi$. For more details see Refs. [24–27].

1. Two-dimensional crystal growth

In this section, first we wish to obtain the linear evolution of the two-dimensional perturbation amplitudes ζ_n of a crystal growing interface. For a general m-fold anisotropy we have $\tau(\theta) = 1 - (m^2-1)\nu_m \cos(m\theta)$, where ν_m is the strength of the anisotropy [26,28,29]. In addition, we consider that ν_m is of the same order of ζ_n such that the product $\nu\zeta$ can be neglected [26,28]. Keeping terms up to the first order in ζ in the system of Eqs. (7), and Fourier transforming, we obtain the equation of motion for the perturbation amplitude [26,28]

$$\dot{\zeta}_n = \lambda(n,R,\dot{R})\zeta_n + \delta_{nm}\frac{2\nu_m}{R^2}m(m^2-1), \tag{8}$$

where

$$\lambda(n,R,\dot{R}) = \frac{\dot{R}}{R}(n-1) - \frac{2}{R^3}n(n^2-1) \tag{9}$$

with δ_{nm} being the Kronecker delta function. In addition, the rate of area growth and the far-field temperature are described as

$$J(t) = R\dot{R} \quad \text{and,} \quad T_\infty(t) = -J(t)\log\left(\frac{R_\infty}{R}\right) - \frac{1}{R}, \tag{10}$$

respectively. In Eq. (10) R_∞ is the radius of a large domain containing the crystal.

To apply the variational method described in Sec. II A, first we obtain the mode of maximum growth-rate $n_{\max} \approx R\dot{R}^{1/2}/\sqrt{6}$ by setting $d\lambda(n,R,\dot{R})/dn = 0$. In this calculation, we assume that the crystal has an isotropic surface tension, so that we neglect the term involving the Dirac delta function in the Eq. (8). This point will be addressed in the discussion of Fig. 2. In this framework, note that the solution for Eq. (8) is given by Eq. (3). Substituting $n_{\max}$ in $\lambda(n,R,\dot{R})$ we have

$$\lambda(R,\dot{R}) \approx \frac{2}{3\sqrt{6}}\dot{R}^{3/2} - \frac{\dot{R}}{R}. \tag{11}$$

Here we assume that $R^2\dot{R}/2 \gg 1$, consistently with Refs. [26,27]. Substituting the expression for $\lambda(R,\dot{R}) = \lambda(n_{\max},R,\dot{R})$ into Eq. (6) we get a very simple differential equation $\ddot{R} = 0$. The solution of such an equation is

$$R(t) = R_0 + \frac{(R_f - R_0)}{t_f}t, \tag{12}$$

where R_0 and R_f are the initial and final unperturbed radii of the crystal, respectively, and t_f is the time required to grow the crystal. From Eqs. (10) and (12) we finally have

$$J(t) = \frac{(R_f - R_0)}{t_f}\left[R_0 + \frac{(R_f - R_0)}{t_f}t\right] \tag{13}$$

and

$$T_\infty(t) = -V(R_0 + Vt)\log\left(\frac{R_\infty}{R_0 + Vt}\right) - \frac{1}{R_0 + Vt}, \tag{14}$$

which describe how the heat flux and the far-field temperature must vary in time in order to minimize the deformations at the crystal interface. In Eq. (14), $V = (R_f - R_0)/t_f$ is the unperturbed interface velocity.

It is worth commenting that our interface stabilization procedure, which uses variational calculus, is distinct from the so-called "feedback control" method utilized by Savina *et al.* [39]. Reference [39] focuses on the possibility of suppressing the morphological instability in directional solidification of a binary liquid. The feedback control stabilization is achieved via external heating of the melt localized near the mel t-crystal interface, where the heating parameters depend on the shape of the interface. On the other hand, our variational scheme focuses on searching for the precise functional form that describes how the far-field temperature must vary in time in order to minimize the perturbation amplitudes at the melt-crystal interface. Another important difference is that our protocol only works for radial growing interfaces (where the growth rate is time dependent), while the feedback control performed in [39] was successfully applied to a rectangular solidification geometry. Mathematically, a fundamental difference between these two approaches is the fact that in feedback control

there exists a contribution of the external heating of the melt in the first expression in the system of Eqs. (7). Besides, we would have to utilize a more sophisticated theory if we wanted to consider the solidification of a binary liquid as examined in Ref. [39]. Therefore, the feedback control is much more involved than our protocol, and has a different physical mechanism.

We proceed by examining the suitability of the interface stabilization process based on the optimal heat flux (13). For a given R_f and t_f, the usual crystal growth problem considers a constant heat flux

$$J_0 = \frac{\left(R_f^2 - R_0^2\right)}{2t_f}. \tag{15}$$

We wish to compare the dynamic behavior and the resulting interface morphologies obtained by using the constant heat flux (15) and the ideal flux (13) at $t = t_f$. Notice from Eq. (15) that the relevant set of parameters to be fixed in the controlling mechanism could be either R_f and t_f, or J_0 and t_f.

The linear stability results of this section are obtained by utilizing dimensionless parameter values consistent with those used in [26,27]. In Fig. 1, we set $R_0 = 1$, $R_f = 200$, and $t_f = 2000$. This figure plots the amplitudes given by Eq. (3) divided by R_f at $t = t_f$, for the optimal heat flux ζ_n/R (solid curve) [which uses Eq. (13)], and for the equivalent constant flux situation ζ_n^0/R (dashed curve) [which utilizes Eq. (15)] as functions of the wave number n. By inspecting Fig. 1 we observe a very significant reduction of the final perturbation amplitudes for the ideal heat flux case. The physical explanation for the success of the ideal stabilization protocol [Eq. (13)] rests on the fact that initially the heat flux is sufficiently small, so that propagation of a sizable unperturbed front is possible. As time progresses the heat flux increases considerably, but since it occurs at a large interfacial radius, the flux is no longer able to promote a significant destabilization of the propagating boundary. This means that the onset of instability is delayed, and when it eventually takes place disturbances arise with a reduced growth rate.

The efficacy of the minimization mechanism can be more clearly visualized in Fig. 2, where we plot the linear evolution of the interfaces for constant heat flux (15) [Figs. 2(a) and 2(c)], and ideal heat flux (13) [Figs. 2(b) and 2(d)]. These linear patterns have the same initial conditions (including the random phases attributed to each mode), and 40 Fourier modes have been considered. The interfaces are plotted in intervals of $t_f/5$. In Figs. 2(a) and 2(b) anisotropy effects are neglected, and we set $R_0 = 1$, $R_f = 200$, and $t_f = 2000$. On the other hand, the effects of anisotropy are included in Figs. 2(c) and 2(d) for $m = 5$ and ν_m considered as having the same order of magnitude as the initial perturbation amplitude [Eq. (8)]. In addition, we take $R_0 = 1$, $R_f = 170$, and $t_f = 2000$. It is evident that finger formation is markedly suppressed on the interfaces shown in the panels on the right. Recall that in the calculation of the optimal heat flux, we neglected anisotropy effects. However, as we can see in Figs. 2(c) and 2(d), our controlling protocol works very well even in the presence of anisotropy. Contrary to what is shown in Figs. 2(a) and 2(c), the interfaces in Figs. 2(b) and 2(d) are evenly spaced due to the constancy of the unperturbed interfacial velocity.

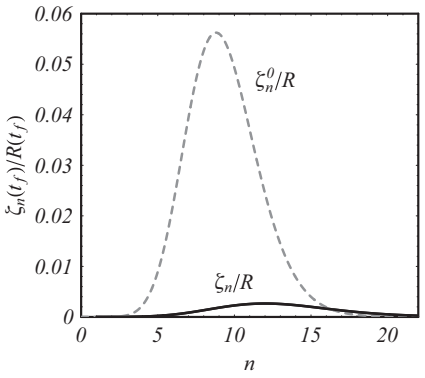

FIG. 1. Perturbation amplitudes given by Eq. (3) divided by R_f at $t = t_f$, for the optimal heat flux ζ_n/R (solid curve), and for the equivalent constant flux situation ζ_n^0/R (dashed curve) as functions of the wave number n.

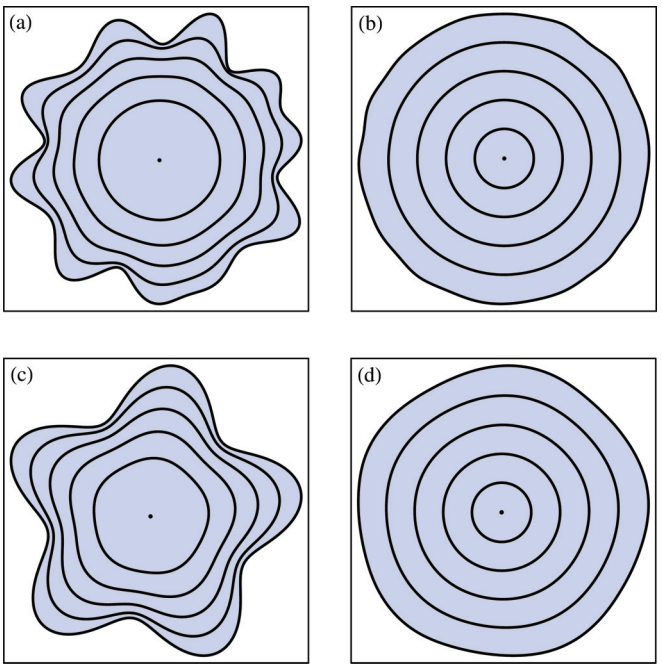

FIG. 2. (Color online) Linear time evolution of the interfacial patterns formed during constant heat flux [(a) and (c)], and optimal flux [(b) and (d)]. Anisotropy effects are neglected in (a) and (b), and taken into account in (c) and (d) for $m = 5$.

It is important to examine the adequacy of our variational protocol when one considers a longer time evolution of the crystal-melt interface. To address this point, in Fig. 3 we plot the maximum amplitude for the constant heat flux situation divided by the maximum amplitude calculated by using the optimal heat flux $[\zeta^0(t_f)/\zeta(t_f)]$, as a function of the final time t_f, for two values of J_0. From Fig. 3 we verify that the ratio $\zeta^0(t_f)/\zeta(t_f)$ grows when t_f is increased, and when larger values of J_0 are considered. We conclude that when we use the ideal heat flux the interface perturbations still remain significantly smaller than the ones obtained by the equivalent constant flux situation, even when higher constant heat fluxes and longer times are considered. These findings are reassuring, and point to the effectiveness of our controlling protocol at

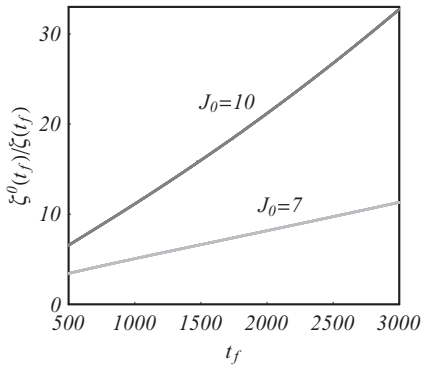

FIG. 3. Amplitude ratio $\zeta^0(t_f)/\zeta(t_f)$ as a function of t_f for $J_0 = 7, 10$. Here $\zeta^0(t_f)$ ($\zeta(t_f)$) denotes the maximum amplitude for constant (optimal) heat flux at $t = t_f$.

longer times. We stress that the type of behavior illustrated in Fig. 3 for the ratio $\zeta^0(t_f)/\zeta(t_f)$ over time has been also verified to all other systems studied in this work.

2. *Three-dimensional crystal growth*

Now, we focus on controlling fingering instabilities in a quasistatic growth of a three-dimensional solid in a supercooled liquid [24,25]. Similar to what we did in the two-dimensional situation, the three-dimensional interface evolves according to

$$\mathcal{R}(\theta,\phi,t) = R(t) + \zeta(\theta,\phi,t), \tag{16}$$

where now θ is the polar angle, ϕ the azimuthal angle, $\zeta(\theta,\phi,t)$ represents the surface perturbation in spherical coordinates, and $R = R(t)$ is the time-dependent unperturbed radius of the interface. We write $\zeta(\theta,\phi,t)$ in terms of the spherical harmonics

$$\zeta(\theta,\phi,t) = \sum_{l=1}^{\infty}\sum_{m=-l}^{l} \zeta_{lm}(t) Y_{lm}(\theta,\phi), \tag{17}$$

with $\zeta_{lm}(t)$ the spherical harmonic amplitudes. In addition, the heat flux is related with the unperturbed radius by [24,25]

$$J(t) = R^2\dot{R} + O(\zeta/R)^2. \tag{18}$$

By using the system of equations (7) and following similar procedures as those of the two-dimensional case, the linear evolution of the interface is describe as [24,25] $\dot{\zeta}_{lm}(t) = \lambda(l)\zeta_{lm}(t)$, where

$$\lambda(l,R,\dot{R}) = \frac{\dot{R}}{R}(l-1) - \frac{1}{R^3}(l+2)(l-1)(1+2l) \tag{19}$$

is the three-dimensional linear growth rate. Here the anisotropy effects are neglected. Since the growth rate does not depend on mode m we can apply the variational protocol described in Sec. II A. Despite the three-dimensional extension of the problem, and the clear difference between Eqs. (9) and (19), the variational method yields the linearly time-dependent Eq. (12). However, from Eq. (18) one can see that now we have a quadratically time-dependent profile for the optimal heat flux,

$$J(t) = \frac{(R_f - R_0)}{t_f}\left[R_0 + \frac{(R_f - R_0)}{t_f}t\right]^2. \tag{20}$$

The far-field temperature can be obtained by the relation $T_\infty(t) = -R(t)\dot{R}(t) - 2/R(t)$ [24,25], plus Eq. (18).

As we did in Sec. II B 1, we compare the resulting interface morphologies obtained by using the constant heat flux with R_0 and R_f fixed

$$J_0 = \frac{\left(R_f^3 - R_0^3\right)}{3t_f}, \tag{21}$$

and the optimal flux (20) at $t = t_f$. The stabilization of the interface obtained by the employment of the variational protocol is illustrated in Fig. 4, where we plot the resulting interface for constant heat flux (21) [left panel of Fig. 4] and ideal heat flux (20) [right panel of Fig. 4]. These linear, three-dimensional patterns have the same initial conditions (including the random phases attributed to each mode), and 18 modes have been considered. We set $R_0 = 1$, $R_f = 11.6$, and $t_f = 1.5$. From Fig. 4 it is clear that the minimization method is also successfully achieved for three-dimensional crystal growth: the bumpy interface depicted on the left is replaced by the smooth spherical surface on the right, when the optimal procedure is put into action.

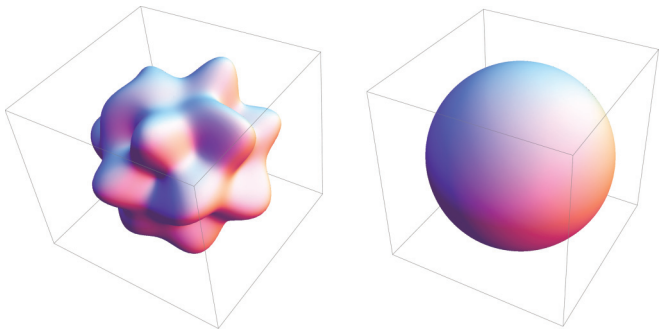

FIG. 4. (Color online) Resulting interfacial patterns at $t = t_f$ by utilizing the constant heat flux (left panel), and optimal heat flux (right panel).

C. Minimization of instabilities in the electric discharge process

In this section we focus on the minimization of the interface instability in the electric discharge problem. This system is well described by a hydrodynamic approximation [33], where stabilizing forces act in the front due to electron diffusion, and destabilizing forces due to electric field tend to increase any disturbances at the interface. In the limit of small electron diffusion $D \ll 1$, a contour-dynamics model have been utilized in Refs. [34–36]. The model describes an interface, with a negative charge density σ, separating a plasma region from a neutral gas. The interface motion is governed by the following dimensionless equations:

$$\begin{aligned} v_N &= -E_v^+ + 2\sqrt{D\alpha(|E_v^+|)} - D\kappa, \\ \frac{\partial\sigma}{\partial t} + \kappa v_N\sigma &= -\frac{E_v^-}{\rho} - j_v^-. \end{aligned} \tag{22}$$

In Eqs. (22), v_N is the normal velocity of the interface, κ is twice the mean interface curvature, E_v^+ (E_v^-) is the normal component of the electric field calculated inside (outside) the plasma, j_v^- is the current density coming from the ionized region to its boundary, ρ is related to the resistivity of the plasma, and $\alpha(x) = x\exp(-1/x)$. For further details we refer the reader to Refs. [34–36].

1. Two-dimensional electric discharge

We can describe the two-dimensional electric discharge interface by Eqs. (1) and (2), and as in Refs. [34–36] we can consider the limit of very high conductivity $1/\rho \gg 1$. To obtain the linear evolution of ζ_n we keep terms up to the first order in ζ in the system of Eqs. (22), and Fourier transform. From this calculation, we get Eq. (3) for the perturbation amplitude with the growth rate given by [34,35]

$$\lambda(n,R,\dot{R}) = \frac{\dot{R}}{R}(n-1) - \frac{\epsilon}{R^2}(n^2-1) - \frac{\sqrt{\epsilon\alpha_0}}{R}\left(1+\frac{2\pi R}{|Q(t)|}\right)(n-1). \quad (23)$$

In Eq. (23), $Q(t) = \int_0^t I(t)dt$, where $I(t)$ is a electric current carried by an insulated wire inside the plasma, $\alpha_0 = \alpha(|Q(t)|/2\pi R)$, and $\epsilon \equiv D$. The term including α_0 in Eq. (23) represents the effects of Townsend expression for impact ionization [34,40,41]. Moreover, we assume the limit used in Ref. [35] [their Eq. (34)]

$$R \ll \frac{|Q(t)|}{4\pi\sqrt{\epsilon\alpha(|Q(t)/2\pi R|)}} \quad \text{and} \quad \epsilon \ll 1 \quad (24)$$

such that the charge $Q(t)$ is related to unperturbed radius of the front by

$$Q(t) \approx -2\pi R\dot{R}. \quad (25)$$

Proceeding similarly as we did in Sec. II B, the mode of maximum growth rate can be written as $n_{\max} = R\dot{R}/(2\epsilon)$. For simplicity, we assume α_0 very small so that we can neglect the term containing $\sqrt{\epsilon\alpha_0}$ in the growth rate (23) (see Refs. [34,35]). Substituting $n_{\max}$ into the Eq. (23) we have the linear growth rate

$$\lambda(R,\dot{R}) = \frac{\dot{R}^2}{4\epsilon} - \frac{\dot{R}}{R} + \frac{\epsilon}{R^2}. \quad (26)$$

Finally, utilizing the Euler-Lagrange equation (6) with Eq. (26) we obtain

$$\ddot{R}R^3 = -4\epsilon^2. \quad (27)$$

The solution of this nonlinear differential equation is

$$R(t) = \sqrt{(C_1 t + C_2)^2 - 4\left(\frac{\epsilon}{C_1}\right)^2}, \quad (28)$$

where C_1 and C_2 are constants to be determined by the initial and final conditions of R: $R(0) = R_0$ and $R(t_f) = R_f$.

However, in the limit of low electric diffusion $\epsilon^2 \ll 1$, as we assumed at the beginning of this section, Eq. (27) becomes the same simple differential equation as we have seen in the crystal growing problem: $\ddot{R} = 0$. Therefore, the solution that minimizes the perturbation amplitude at the interface in the electric discharge process is also given by Eq. (12). Finally, from Eq. (25) we get the controlling charge and electric current

$$Q(t) = -2\pi\frac{(R_f - R_0)}{t_f}\left[R_0 + \frac{(R_f - R_0)}{t_f}t\right], \quad (29)$$

$$I = -2\pi\left[\frac{(R_f - R_0)}{t_f}\right]^2. \quad (30)$$

From Eq. (29) we see that the electric charge carried by an insulated wire inside the plasma must vary linearly with time in order to minimize the deformations at the plasma interface.

Similar to what we did in Sec. II B we go on and test the efficiency of the variational protocol based on the optimal electric charge (29). For a given R_f and t_f, the usual electric discharge problem considers the constant charge

$$Q_0 = -\frac{\pi\left(R_f^2 - R_0^2\right)}{t_f}. \quad (31)$$

Our goal is to contrast the interface behavior which results from the use of the constant charge (31) and the optimal charge (29) at $t = t_f$. Here we utilize dimensionless parameter values consistent with those used in Refs. [34,35]. In addition, we set $\epsilon = 0.03$, $R_0 = 0.14$, $R_f = 0.44$, and $t_f = 0.08$. As we did in the preceding section, first we plot in Fig. 5 the amplitudes given by Eq. (3) divided by R_f at $t = t_f$, for the optimal charge ζ_n/R (solid curve) [Eq. (29)], and for the equivalent constant charge situation ζ_n^0/R (dashed curve) [Eq. (31)] as functions of the wave number n. By examining this figure it is evident that our variational method results in significantly diminished perturbation of the ionization fronts in the electric discharge problem.

These predictions are reinforced by the linear interfacial evolution illustrated in Fig. 6: Figs. 6(a) and 6(c) are plotted for constant charge (31), while Figs. 6(b) and 6(d) relate to the ideal charge situation (29). The plots show in the first row [Figs. 6(a) and 6(b)] does not include the α_0 term in the growth rate [35], and the patterns shown in the second row [Figs. 6(c) and 6(d)] adds its influence [34]. By observing Fig. 6 it is

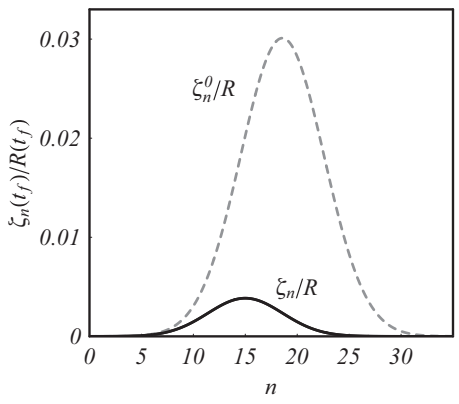

FIG. 5. Perturbation amplitudes given by Eq. (3) divided by R_f at $t = t_f$, for the optimal electric charge ζ_n/R (solid curve), and for the equivalent constant charge situation ζ_n^0/R (dashed curve) as functions of the wave number n.

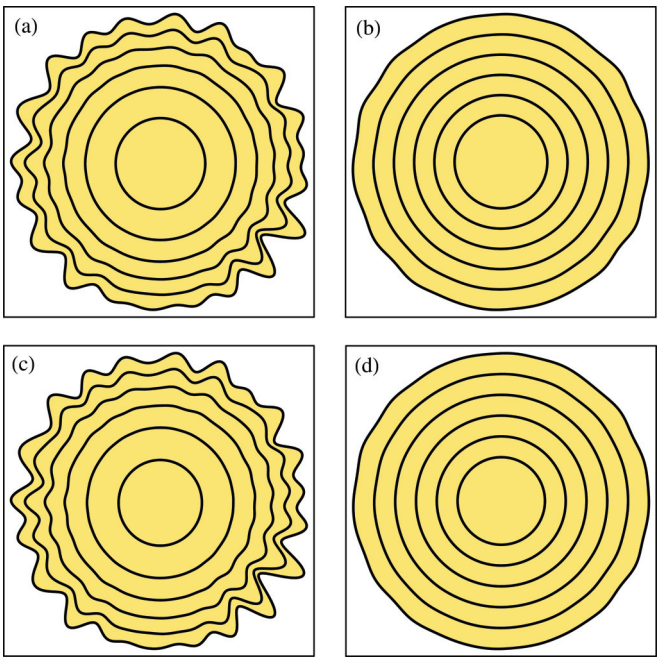

FIG. 6. (Color online) Linear time evolution of the interfacial patterns formed during constant charge [(a) and (c)], and optimal charge [(b) and (d)]. The effects of the α_0 term in the linear dispersion (23) are neglected in (a) and (b) [where $R_0 = 0.14$, $R_f = 0.44$, and $t_f = 0.08$], and considered in (c) and (d) [where $R_0 = 0.14$, $R_f = 0.47$, and $t_f = 0.08$]. These linear patterns have the same initial conditions (including the random phases attributed to each mode), and 40 Fourier modes have been considered. The interfaces are plotted in intervals of $t_f/5$. We take $\epsilon = 0.03$.

clear that our variational method works nicely regardless of the consideration or not of the α_0 term.

2. *Three-dimensional electric discharge*

In order to minimize a three-dimensional electric discharge we follow similar steps as those described in Sec. II B 2. The interface position is described by Eq. (16), and the perturbation amplitudes are written in terms of the spherical harmonics (17). Now, by assuming the limit used in Ref. [36] [their Eq. (A6)] the unperturbed radius and the electric charge are related by

$$Q(t) \approx -4\pi R^2 \dot{R}. \tag{32}$$

By using the system of Eqs. (22) in the limit of very high conductivity, and keeping terms up to the first order in ζ, we obtain a three-dimensional linear growth rate given by [36]

$$\lambda(l, R, \dot{R}) = \frac{\dot{R}}{R}(l-1) - \frac{\epsilon}{R^2}(l+2)(l-1). \tag{33}$$

For simplicity, as we did previously, we assume α_0 very small so that we can neglect the terms of the Townsend expression for impact ionization [34,36,40,41] in the growth rate (33). By applying the variational protocol for this system, the optimal evolution for the unperturbed radius is

$$R(t) = \sqrt{(\mathrm{C}_1 t + \mathrm{C}_2)^2 - 6\left(\frac{\epsilon}{\mathrm{C}_1}\right)^2}, \tag{34}$$

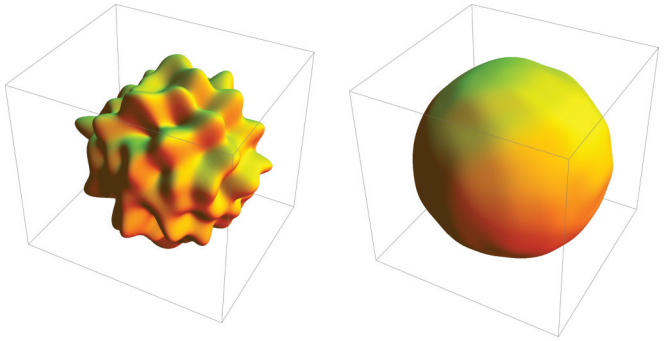

FIG. 7. (Color online) Resulting interfacial patterns at $t = t_f$ by utilizing the constant electric charge (left panel), and the optimal charge (right panel).

where C_1 and C_2 are constants to be determined by the initial and final conditions of R: $R(0) = R_0$ and $R(t_f) = R_f$. From Eq. (32) the optimal electric charge in the limit of small ϵ is

$$Q(t) = -4\pi \frac{(R_f - R_0)}{t_f}\left[R_0 + \frac{(R_f - R_0)}{t_f} t\right]^2. \tag{35}$$

Note that while the two-dimensional optimal charge [Eq. (29)] varies linearly in time, in three dimensions the optimal charge evolves as $Q(t) \sim t^2$.

Figure 7 illustrates the suitability of the protocol stabilization by comparing the resulting interface morphologies obtained by using the constant charge

$$Q_0 = -\frac{4\pi\left(R_f^3 - R_0^3\right)}{3t_f} \tag{36}$$

(left panel of Fig. 7) and the optimal charge (35) (right panel of Fig. 7) at $t = t_f$. The resulting interface have the same initial conditions (including the random phases attributed to each mode), and 18 modes have been considered. We set $\epsilon = 0.03$, $R_0 = 0.13$, $R_f = 0.43$, and $t_f = 0.16$. The spiky three-dimensional structure obtained under constant charge, is replaced by an almost perfect sphere when the optimal charge is used.

III. CONCLUDING REMARKS

The ability to control interfacial instabilities in crystal growth and electric discharge phenomena is a subject of considerable relevance to science and technology. In the conventional version of these problems, interface destabilization leads to the formation of complex pattern morphologies resulting in the emergence of dendritic and branched treelike structures.

One challenging question in the study of the Mullins-Sekerka and electric breakdown instabilities pertains to what would be the optimal way to provide growth in these systems, in such a way that the interfacial deformations would be minimized. In this work, we used an analytical variational scheme to systematically search for ideal conditions that would promote growth with minimum interface disturbances. This has been done by tackling both the two-dimensional and three-dimensional versions of the problems. By employing this variational technique we have been able to find the ideal functional form for heat flux in the Mullins-Sekerka case,

and for the optimal electric charge in the electric discharge problem in which interfaces evolve, but are constrained to present minimal perturbation amplitudes.

A possible extension of this work could be the investigation of fully nonlinear stages of the dynamics (for both two-dimensional and three-dimensional situations) through computer simulations and experiments. This could offer ways to test our theoretical predictions, and to examine how our variational controlling method would alter the morphology of the emerging patterns in crystal growth and electric discharge processes.

ACKNOWLEDGMENTS

We thank CNPq for financial support through the program "Instituto Nacional de Ciência e Tecnologia de Fluidos Complexos (INCT-FCx)," and FACEPE through PRONEM Project No. APQ-1415-1.05/10.

[1] D. W. Thompson, *On Growth and Form* (Cambridge University Press, Cambridge, 1944).
[2] P. S. Stevens, *Patterns in Nature* (Little Brown, Boston, 1974).
[3] P. Ball, *The Self-Made Tapestry: Pattern Formation in Nature* (Oxford University Press, New York, 2001).
[4] H. Meinhardt, *Models of Biological Pattern Formation* (Academic, New York, 1982).
[5] J. Binney and S. Tremaine, *Galactic Dynamics* (Princeton University Press, Princeton, 1987).
[6] S. Chandrasekhar, *Hydrodynamic and Hydromagnetic Stability* (Oxford University, London, 1961).
[7] B. Chalmers, *Principles of Solidification* (Wiley, New York, 1964).
[8] L. A. Segel, *Mathematical Models of Molecular and Cellular Biology* (Cambridge University Press, Cambridge, 1980).
[9] P. G. Saffman and G. I. Taylor, Proc. R. Soc. London Ser. A **245**, 312 (1958).
[10] H. S. Hele-Shaw, Trans. R. Inst. Naval Arch. **40**, 21 (1898).
[11] For review papers see, for instance, G. M. Homsy, Annu. Rev. Fluid Mech. **19**, 271 (1987); K. V. McCloud and J. V. Maher, Phys. Rep. **260**, 139 (1995); J. Casademunt, Chaos **14**, 809 (2004).
[12] S. B. Gorell and G. M. Homsy, SIAM J. Appl. Math. **43**, 79 (1983); J. P. Stokes, D. A. Weitz, J. P. Gollub, A. Dougherty, M. O. Robbins, P. M. Chaikin, and H. M. Lindsay, Phys. Rev. Lett. **57**, 1718 (1986).
[13] B. Jha, L. Cueto-Felgueroso, and R. Juanes, Phys. Rev. Lett. **106**, 194502 (2011).
[14] X. Cheng, L. Lu, A. Patterson, H. M. Jaeger, and S. R. Nagle, Nat. Phys. **4**, 234 (2008).
[15] H.-Y. Chu and H.-K. Lee, Phys. Rev. Lett. **107**, 225001 (2011).
[16] A. C. Callan-Jones, J.-F. Joanny, and J. Prost, Phys. Rev. Lett. **100**, 258106 (2008).
[17] C. Blanch-Mercader and J. Casademunt, Phys. Rev. Lett. **110**, 078102 (2013).
[18] J. S. Langer, Rev. Mod. Phys. **52**, 1 (1980).
[19] For classic reviews in dendritic growth see, *Dynamics of Curved Fronts*, edited by P. Pelcé (Academic, Boston, 1988); D. A. Kessler, J. Koplik, and H. Levine, Adv. Phys. **37**, 255 (1988); J. S. Langer, in *Chance and Matter*, Proceedings of the Les Houches Summer School Section 46, edited by J. Souletie, J. Vannimenus, and R. Stora (North-Holland, Amsterdam, 1986).
[20] W. W. Mullins and R. F. Sekerka, J. Appl. Phys. **34**, 323 (1963).
[21] W. W. Mullins and R. F. Sekerka, J. Appl. Phys. **35**, 444 (1964).
[22] S. R. Coriell and R. L. Parker, J. Appl. Phys. **36**, 632 (1965).
[23] L. N. Brush and R. F. Sekerka, J. Cryst. Growth **96**, 419 (1989).
[24] V. Cristini and J. S. Lowengrub, J. Cryst. Growth **240**, 267 (2002).
[25] V. Cristini and J. S. Lowengrub, J. Cryst. Growth **266**, 552 (2004).
[26] S. Li, J. S. Lowengrub, P. H. Leo, and V. Cristini, J. Cryst. Growth **267**, 703 (2004).
[27] S. Li, J. S. Lowengrub, P. H. Leo, and V. Cristini, J. Cryst. Growth **277**, 578 (2005).
[28] S. Li, J. S. Lowengrub, and P. H. Leo, Physica D **208**, 209 (2005).
[29] Y. Saito, *Statistical Physics of Crystal Growth* (World Scientific, Singapore, 2005).
[30] Y. P. Raizer, *Gas Discharge Physics* (Springer, Berlin, 1991).
[31] H. Raether, *Electron Avalanches and Breakdown in Gases* (Butterworths, London, 1964).
[32] V. P. Pasko, Nature (London) **423**, 927 (2003).
[33] A. N. Lagarkov and I. M. Rutkevich, *Ionization Waves in Electron Breakdown on Gases* (Springer-Verlag, New York, 1994).
[34] M. Arrayás, M. A. Fontelos, and C. Jimenéz, Phys. Rev. E **81**, 035401(R) (2010).
[35] M. Arrayás and M. A. Fontelos, Phys. Rev. E **84**, 026404 (2011).
[36] M. Arrayás, M. A. Fontelos, and U. Kindelán, Phys. Rev. E **86**, 066407 (2012).
[37] E. O. Dias, E. Alvarez-Lacalle, M. S. Carvalho, and J. A. Miranda, Phys. Rev. Lett. **109**, 144502 (2012).
[38] J. A. Miranda and M. Widom, Physica D **120**, 315 (1998).
[39] T. V. Savina, A. A. Nepomnyashchy, S. Brandon, D. R. Lewin, and A. A. Golovin, J. Cryst. Growth **240**, 292 (2002).
[40] U. Ebert, W. van Saarloos, and C. Caroli, Phys. Rev. Lett. **77**, 4178 (1996).
[41] U. Ebert, W. van Saarloos, and C. Caroli, Phys. Rev. E **55**, 1530 (1997).